RSC Advances

PAPER

View Article Online
View Journal | View Issue

Cite this: *RSC Adv.*, 2016, **6**, 2450

3D printing of Al_2O_3 photonic crystals for terahertz frequencies

Carmen R. Tubío,[a] José A. Nóvoa,[b] Jorge Martín,[b] Francisco Guitián,[a] José R. Salgueiro*[b] and Alvaro Gil*[a]

Received 29th October 2015
Accepted 23rd December 2015

DOI: 10.1039/c5ra22737b

www.rsc.org/advances

Reported here is the fabrication and characterization of a three-dimensional photonic crystal for terahertz frequencies based on 3D printing of Al_2O_3. Specific inks containing Al_2O_3, the material required for the structure, are synthesized with the viscosity and rheological properties necessary to be extruded through nozzles of micrometric section. The process is completed by a thermal sintering to obtain compact structures. SEM measurements are performed to evaluate the quality of the structures and measure the geometrical parameters. Finally, the presence of the band gap is demonstrated by THz time-domain spectroscopy.

Introduction

Optoelectronic devices for terahertz (THz) frequencies such as filters, detectors, lasers and waveguides, are of considerable interest because of their potential applications in structural analysis of materials and complex molecules,[1] medical and biological imaging,[2] security sectors,[3] dopant density measurement and pollution gases detection[4,5] among others. In order to fabricate functional devices where the control of THz waves is required, photonic crystals (PCs)[6,7] presenting a complete photonic band gap (PBG) play a crucial role since propagation of electromagnetic waves is forbidden for all wave vectors in such a band. While the fabrication of PCs was mainly conducted at microwave,[8] infrared[9] and visible[10] bands, the study of PCs for the THz band is one of the less explored.[11] Most studies of PCs in this spectrum band have been focused on the development of passive devices such as filters[12] and waveguides,[13] and on the integration of PCs with active devices such as quantum-cascade lasers.[14] Further progress towards the development of devices operating at THz frequencies is driven by the need of fabrication of optimized PCs with a complete PBG at this spectrum band.

It is well known that the efficiency of functional photonic devices at the operational frequency range is strongly dependent on the properties of materials, *i.e.* their dielectric constant, and the symmetry and lattice constant of the periodic structure. Al_2O_3 is a particularly attractive candidate for potential optical devices because this oxide shows a high optical transparency and a high dielectric constant in the THz band.[15] Various techniques such as laser chemical vapour deposition[16] and stereolithography[17] have been used to fabricate three-dimensional Al_2O_3 PC devices for THz operation. However, those methods are technically complicated and also present difficulties associated to the use of laser sources with critical processing.[18] As an alternative, here we demonstrate that high-quality Al_2O_3 PCs structures operating at THz frequencies can be easily constructed using a 3D printing technique. For this fabrication method, concentrated inks with tailored rheological properties can be extruded through nozzles and deposited onto a substrate to yield complex 3D structures on the micrometer to millimeter scale in a layer-by-layer sequence.[19] Significant progress in this technique has demonstrated a great potential for developing functional devices with potential applications as photonic crystals,[20] electronic components[21] and tissue engineering elements.[22]

Herein, we present the fabrication and characterization of an Al_2O_3 structure with potential to fabricate photonic THz devices for the 0.1–10 THz band. The designed 3D lattice, which has been optimized for the THz band, consists of a woodpile structure that is composed of dielectric rods stacked in a periodic layer-by-layer sequence and exhibits a symmetry of a face-centred-tetragonal (fct) lattice.[9] This structure is defined by two parameters, the diameter of rods w and the rod spacing d. The distance between the centres of adjacent layers is w, with a stacking sequence that repeats itself every four layers and with adjacent layers rotated by 90 degrees. Additionally, alternate layers are shifted half a period, *i.e.* a distance $d/2$. In such a way the primitive cell has a tetragonal shape with dimension d in both directions of the layers plane and $a = 4w$ in the perpendicular direction. By controlling the composition of the ink and the processing parameters in the printing process, it is possible to generate this 3D woodpile periodic structure with the specified dimensions for the THz operation range. After printing,

[a]*Instituto de Cerámica, Universidade de Santiago de Compostela, Santiago de Compostela, 15782, Spain. E-mail: alvaro.gil@usc.es*

[b]*Departamento de Física Aplicada, Universidade de Vigo, Ourense, 32004, Spain. E-mail: jrs@uvigo.es*

the structure was dried and calcined at high temperature to induce a sintering process that increases its density and mechanical strength. Finally, in order to check the presence of the bandgap a test is conducted measuring the transmittance of the sample in the low THz band using the time-domain spectroscopy technique (THz-TDS), and comparing the results to the simulations carried out by the plane wave expansion method (PWE).

Experimental

Ink synthesis

An Al_2O_3 suspension (30 vol%) was prepared by adding 91.8 g of Al_2O_3 powder (0.5 μm mean particle size and density of 3.98 g mL^{-1}, Almatis GmbH, Germany) to 53.8 mL of an aqueous solution of 0.5 wt% of dispersant (Darvan 821A, R.T. Vanderbilt Company Inc., USA). This suspension was ultrasonicated for 30 min (IKA U200S, Germany) to ensure the uniform dispersion of the particles, and then centrifuged at 2500 rpm for 15 min. Afterwards, the concentration of the ink was adjusted to 50 vol% by the elimination of 30.7 mL of the supernatant, and the mixture was homogenized for 2 min in a planetary centrifugal mixer (Thinky ARE-250, Thinky, Japan) at 2000 rpm. Then, 0.13 wt% (based powder) of a viscosity modifier hydroxypropyl methylcellulose (HPMC, viscosity 2600–5600 cP, Sigma-Aldrich) was added to the ink. The resulting suspension was stirred again in the planetary centrifugal mixer for 2 min and was allowed to stand at room temperature for 1 h. Finally, the suspension was gelled by adding the flocculant cationic polyelectrolyte poly(ethylenimine) (PEI, $M_w = 2000$, Sigma-Aldrich) at 0.17 wt% (based powder) and the suspension was again stirred four times at 2000 rpm for 2 min.

Rheological characterization

The rheological properties of the Al_2O_3 ink were conducted at 25 °C using a rotational rheometer (Kinexus pro+, Malvern Instruments, UK) with parallel plates geometry (diameter of 20 mm and gap width of 1 mm). The apparent viscosity was measured at the shear rate range from 0 to 80 s^{-1}. The viscoelastic behaviour of the ink was determined by an oscillatory time sweep experiment. This study provides information about the evolution of the elastic modulus G' with the time. The time sweep is made at a frequency of 1 Hz and a constant stress of 1 Pa. Before every measurement, the ink was subjected to a pre-sheared rate of 1 s^{-1} for 2 min followed by a 10 min equilibrium time to minimize de effect of the ink loading.

Fabrication of the photonic crystal

The 3D structure was designed using a CAD program, and then was performed at 25 °C in air using a robotic deposition apparatus (A3200, Aerotech Inc., USA). The ink was housed in a syringe and tapered with a nozzle (diameter 200 μm, Nordson EFD, Japan). To control the ink flow rate an air powered fluid dispenser Performus VII (Nordson EFD) combined with an air-pressure multiplier-dispensing system (HP7x, Nordson EFD) was used. The applied pressure for extrusion was 14 bar and the velocity fabrication 5 mm s^{-1}. After drying for 24 h, the structure was sintered in a furnace for 2.5 h at a temperature of 1500 °C with a heating rate of 5 °C min^{-1}.

Additionally a solid tablet (without porosity and surface defect) was also fabricated. This tablet consisted of dried Al_2O_3 ink that was uniaxially pressed into a cylindrical cast with 12 mm diameter and 3 mm thickness. Afterwards, the sample was heated using the same thermal treatment than the woodpile structure.

Optical characterization

The spectroscopic measurements were performed using a developed time-domain spectrometer set up. It uses a 810 nm wavelength Ti–Za laser producing pulses of 75 fs with a repetition rate of 80 MHz whose beam is split and directed into two photoconductive antennas (Menlo TERA8-1) to produce and detect the THz radiation. The detected signal is a small current in the range of tenths of nA which is amplified and converted into a voltage by means of a low noise transimpedance amplifier and then isolated from noise by means of a lock-in amplifier to be finally read by a data acquisition card from a computer. The temporal scanning is achieved by delaying one of the beams using a mirror attached to a motorized stage, which is controlled from the same computer to automatize the whole measurement process. On the other hand, the THz radiation from the emitter is precollimated by a silicon hyper-hemispherical lens and then collimated and focused into the sample by a pair of plano-convex TPX polymer lenses. Another set of two plano-convex and hyper-hemispherical lenses are used to direct the output to the receiver.

A stereomicroscope (Olympus, SZX12 Olympus, Japan) and a scanning electron microscope (JEOL 6400, Jeol Ltd., Japan) were used to characterize the morphology of the Al_2O_3 photonic crystal.

Results and discussion

To produce the periodic structures by 3D printing, the composition and rheology of a highly concentrated aqueous colloidal ink (composed of 50 vol% Al_2O_3 powder, deionized water, viscosity modifier and gelling agent) must be controlled. The rheological properties of this aqueous ink (apparent viscosity and elastic modulus) were measured in order to know the flow behaviour and to evaluate whether it was suitable for printing. These measurements were conducted at 25 °C using a rotational rheometer, with parallel plate geometry (diameter 20 mm, gap 1 mm). The apparent viscosity was measured as a function of the shear rate (0–80 s^{-1}). For the time sweep test, elastic modulus G' was monitored as a function of time at a frequency of 1 Hz and a constant stress of 1 Pa (value determined for the linear viscoelastic region of the stress sweep measurement). The dependence of the ink viscosity with the shear rate is shown in Fig. 1a. The ink exhibits pseudoplastic (shear-thinning) rheological behaviour, which is characterized by decreasing viscosity with increasing shear rate. This is the desirable

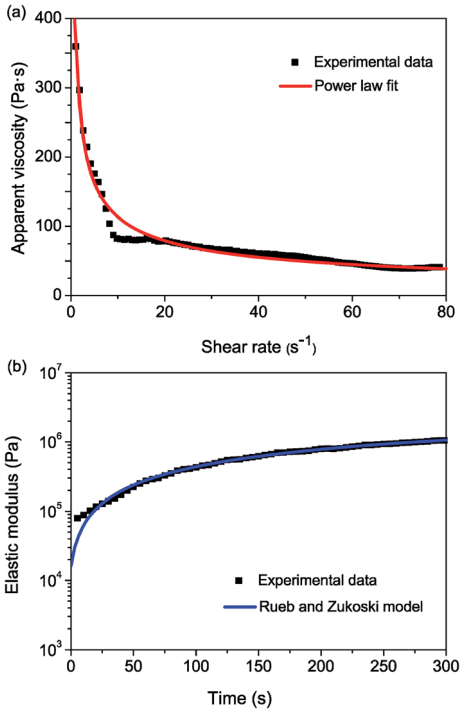

Fig. 1 (a) Apparent viscosity *versus* shear rate of the Al_2O_3 ink at solid loading (50 vol%). The solid line represents the power law model fit. (b) Time evolution of the elastic modulus for the Al_2O_3 ink. The solid line displays the fit to the Rueb and Zukoski model.

behaviour to the extrusion process, enabling the ink to flow through fine nozzles and subsequently holding its shape against the influence of the weight of the structure. Adjusting the experimental data to the power law model:[23]

$$\eta = K\dot{\gamma}^{n-1} \quad (1)$$

where η is the viscosity, K the consistency index, $\dot{\gamma}$ the shear rate and n the flow behaviour index. A good fitting to the model was confirmed ($R^2 = 0.969$) with a consistency index $K = 373.34$ Pa s^n and a flow behaviour index of $n = 0.482$, which was indicative of pseudoplastic behaviour ($0 < n < 1$). Furthermore, we also evaluated the crosslinking kinetics of the ink as it provides useful information about the fact whether the rods retain their cylindrical shape after printing or not. The time sweep test (Fig. 1b) shows a gradual increase of elastic modulus G' with time, due to the formation of the cross-linked network. This dependence is described by the modified Rueb and Zukoski model:[24]

$$G'(t) = (G'_\infty - G'_0)[1 - \exp(\alpha - t)] + G'_0 \quad (2)$$

where G'_∞ is the instantaneous modulus recorded at $t = \infty$, G'_0 the instantaneous modulus recorded at $t = 0$, and α the decay constant. For the Al_2O_3 ink, G'_0 and G'_∞ were 1.6×10^4 Pa and 2.3×10^6 Pa respectively, with a R^2 value of 0.998. Previous studies have determined the minimum ink elasticity to build a 3D periodic structure without deflections in the filamentary rods.[25] Based on this calculation, a minimum G' of 109.59 Pa is required for the conditions given in our study (*i.e.*, ink density $\rho_{ink} = 2.49$ g mL^{-1}, 566 μm rod spacing and 200 μm rod diameter). Our results indicate that the concentrated Al_2O_3 ink (50 vol%) has enough initial elasticity to produce a self-supporting 3D periodic structure.

To fabricate the 3D PC we printed a woodpile structure with 5 unit cells (20 layers), a rod spacing of 566 μm and a rod diameter of 200 μm. Fig. 2 shows the schematic structure of a woodpile with an fct lattice (a) and SEM and optical microscope images of the 3D structure after sintering (b–d). The rod spacing (368 μm) and rod diameter (153 μm) measured in Fig. 2c resulted after a strong reduction regarding to the values before the thermal treatment with a non-uniform contraction along the x and y directions. This shrinkage is a consequence of the sintering process produced at high temperature. The shrinkage corresponds to a 24% and a 35% reduction in rod diameter and spacing, respectively, giving a PC structure with a fct symmetry and a lattice constant of 612 μm ($a = 4 \times 153$ μm). The cross-sectional SEM image (Fig. 2d) of the woodpile structure after the thermal treatment at 1500 °C reveals no morphology change of the sample that retains its initial shape. The surface morphology of a rod is shown as a high-magnification SEM image in Fig. 2d, revealing a good densification of the Al_2O_3 grains due to the controlled sintering process.

In order to check the presence and position of this gap we calculated numerically the band structure of the woodpile for the parameters measured from SEM images (lattice dimensions and rod diameter), as well as the dielectric constants for the background media (air, $\varepsilon = 1$) and Al_2O_3 rods ($\varepsilon = 9.8$).[15] The calculation was done using the MIT Photonic Bandgaps software package, based on the plane wave expansion method.[26] The band diagram is presented in Fig. 3. The scale of wavenumber on the horizontal axis is proportional to the ratio of reciprocal lattice dimensions, *i.e.* $k_x = k_y = 2\pi/d$, $k_z = 2\pi/a$,

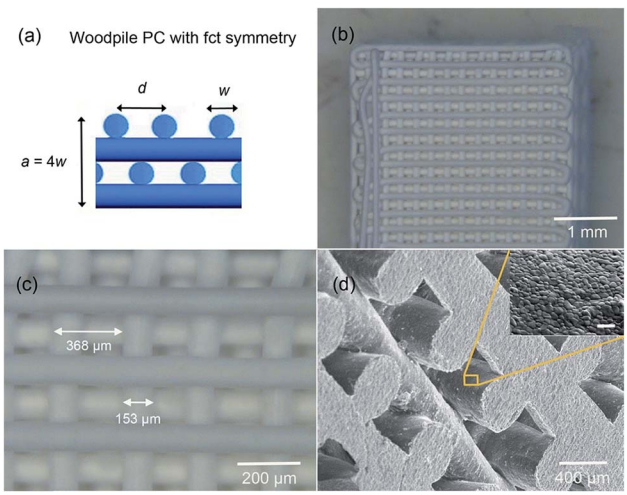

Fig. 2 (a) Schematic cross-view structure of a woodpile with an fct lattice. (b and c) Optical micrographs (top view) at varying magnifications of the Al_2O_3 woodpile structure thermally treated (1500 °C for 2.5 h). (d) Cross-sectional SEM image of sintered structure, the inset shows a surface at higher magnification (scale bar = 2 μm).

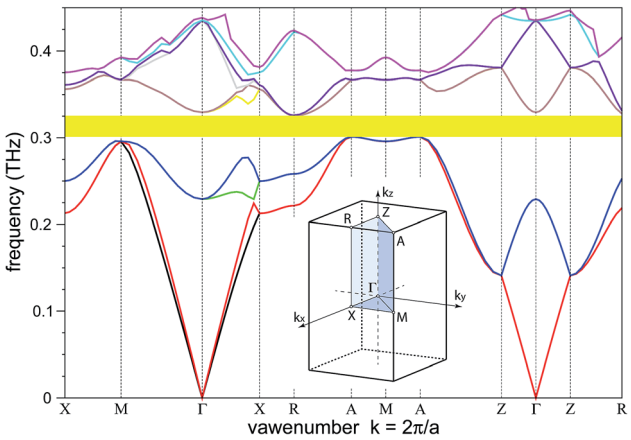

Fig. 3 Band structure for the Al_2O_3 woodpile structure. The shaded area represents the complete band gap (for all crystal directions). Inset: sketch of first Brillouin zone for the tetragonal structure showing the special symmetry points that correspond to the wavenumber values on the horizontal axis of the band diagram.

so that $k_z/k_x = d/a = 368/612 = 0.60$. A sketch (not to scale) of the first Brillouin zone is represented in the inset in order to illustrate the position of the characteristic symmetry points for the tetragonal structure[27] which are also indicated in the wavenumber axis on the band diagram. The band structure shows a full band gap between 4th and 5th bands for the frequency range 0.30–0.32 THz (shaded area) with a relative width of $\Delta w/w_g = 7.63\%$.

We performed transmission measurements of the Al_2O_3 photonic crystal using a terahertz time-domain spectrometer. The system produces short THz pulses (T-rays) which are made to go through the sample and finally detected producing a temporal signal which can be converted into a frequency spectrum *via* a numeric Fourier transform. In the arranged set up,[28,29] the THz beam is focused between emitter and detector at the point where the sample is placed. The transmission spectrum of the free space and a compact tablet sample of sintered Al_2O_3 show a close overlapping (Fig. 4a), which suggest that Al_2O_3 is nearly transparent at such frequency range. In contrast, the woodpile structure exhibits a strong decay in the region 0.25–0.8 THz reaching a value of ~61% respect to the tablet spectrum signal, indicative of the presence of a band gap. This fact is confirmed in Fig. 4b where the transmittance is plotted for both tablet and woodpile samples.

To compare the band structure with the experimental results, we should note that measurements were performed when the woodpile sample was placed with the staking axis parallel to the THz-beam direction, which corresponds to a wave-vector mainly oriented in the Γ–Z direction. The THz radiation impinges on the sample as a cone of rays due to focusing. This means the gap measured experimentally is necessarily broader than the theoretical complete band gap since transmission is restricted to a limited set of incident angles. In Fig. 4b it is appreciated a deep minimum at the position of the full band gap (around 0.3 THz). A comparison

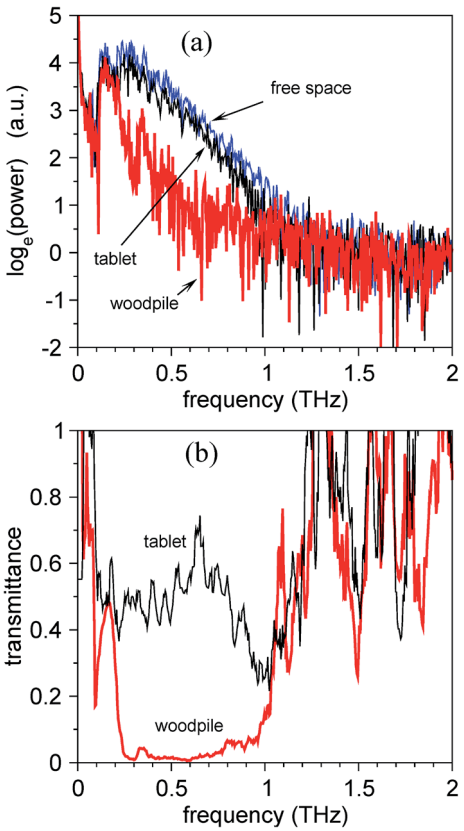

Fig. 4 (a) Measured spectral power as a function of the frequency for the free space, the compact tablet sample of Al_2O_3 and the woodpile structure of Al_2O_3. (b) Transmittance for the tablet and woodpile structure.

between tablet and woodpile curves reveals the relevance of the photonic crystal structure on the transmission of the sample.

Conclusion

In conclusion we have fabricated a 3D terahertz functional structure with tailored geometry by a 3D printing technique. The fabrication uses optimized highly concentrated aqueous Al_2O_3 ink, followed by a sintering process to produce a structure with closed porosity and good mechanical strength. The resulting photonic crystal consists of a woodpile structure with fct symmetry and a lattice constant a = 612 μm. The spectrometric measurements show the presence of a band gap and a comparison with the calculated band diagram demonstrates that the position of the band gap is at the numerically predicted frequency. Due to the versatility of 3D printing technique, those parameters can be easily controlled, offering flexibility for the design of devices operating at the THz frequency band. The results obtained would be valuable for the integration of engineered woodpile structure-based devices.

Acknowledgements

The authors acknowledge funding from the Galician Government under grants No. 10PXIB265118PR and No. 10PXIB383118PR and GPC2015/019.

Notes and references

1 C. L. Strachan, T. Rades, D. A. Newnham, K. C. Gordon, M. Pepper and P. F. Taday, *Chem. Phys. Lett.*, 2004, **390**, 20–24.
2 T. W. Crowe, T. Globus, D. L. Woodlard and J. L. Hesler, *Philos. Trans. R. Soc. London, Ser. A*, 2004, **362**, 365–377.
3 D. L. Woolard, J. O. Jensen, R. J. Hwu and M. S. Shur, *Terahertz science and technology for military and security applications*, World Scientific, Singapore, 2007.
4 A. Redo-Sanchez, G. Salvatella, R. Galceran, E. Roldós, J. A. García-Reguero, M. Castellari and J. Tejada, *Analyst*, 2011, **21**, 1733–1738.
5 D. M. Mittleman, R. H. Jacobsen, R. Neelamani, R. G. Baraniuk and M. C. Nuss, *Appl. Phys. B*, 1998, **67**, 379–390.
6 E. Yablonovitch, *Phys. Rev. Lett.*, 1987, **58**, 2059–2062.
7 S. John, *Phys. Rev. Lett.*, 1987, **58**, 2486–2489.
8 E. Özbay, *J. Opt. Soc. Am. B*, 1996, **13**, 1945–1955.
9 S. Y. Lin, J. G. Fleming, D. L. Hetherington, B. K. Smith, R. Biswas, K. M. Ho, M. M. Sigalas, W. Zubrzycki, S. R. Kurtz and J. Bur, *Nature*, 1998, **394**, 251.
10 A. Frölich, J. Fischer, T. Zebrowski, K. Busch and M. Wegener, *Adv. Mater.*, 2013, **25**, 3588–3592.
11 J. Lott, C. Xia, L. Kosnosky, C. Weder and J. Shan, *Adv. Mater.*, 2008, **20**, 3649–3653.
12 T. D. Drysdale, I. S. Gregory, C. Baker, E. H. Linfield, W. R. Tribe and D. R. S. Cumming, *Appl. Phys. Lett.*, 2004, **85**, 5173.
13 A. L. Bingham and D. Grischkowsky, *Appl. Phys. Lett.*, 2007, **90**, 091105.
14 H. Zhang, L. A. Dunbar, G. Scalari, R. Houdré and J. Faist, *Opt. Express*, 2007, **15**, 16818–16827.
15 N. Ohta, T. Niki and S. Kirihara, *IOP Conf. Ser.: Mater. Sci. Eng.*, 2011, **18**, 072015.
16 M. C. Wanke, O. Lehmann, K. Müller, Q. Wen and M. Stuke, *Science*, 1997, **275**, 1284–1286.
17 H. Kanaoka, S. Kirihara and Y. Miyamoto, *J. Mater. Res.*, 2008, **23**, 1036–1041.
18 W. M. Steen, *Laser Material Processing*, Springer-Verlag, London, 1998.
19 R. B. Rao, K. L. Krafcik, A. M. Morales and J. A. Lewis, *Adv. Mater.*, 2005, **17**, 289–293.
20 E. B. Duoss, M. Twardowski and J. A. Lewis, *Adv. Mater.*, 2007, **19**, 3485–3489.
21 J. J. Adams, E. B. Duoss, T. F. Malkowski, M. J. Motala and B. Y. Ahn, *Adv. Mater.*, 2011, **23**, 1335–1340.
22 S. Eqtesadi, A. Motealleh, P. Miranda, A. Pajares and A. Lemos, *J. Eur. Ceram. Soc.*, 2014, **34**, 107–118.
23 J. Mewis and N. J. Wagner, *Colloidal Suspension Rheology*, Cambridge University Press, New York, 2012.
24 C. J. Rueb and C. F. Zukoski, *J. Rheol.*, 1997, **41**, 197–218.
25 J. E. Smay, J. Cesarano III and J. A. Lewis, *Langmuir*, 2002, **18**, 5429–5437.
26 S. G. Johnson and J. D. Joannopoulos, *Opt. Express*, 2001, **8**, 173–190.
27 M. Lax, *Symmetry principles in solid state and molecular physics*, J. Wiley, New York, 1974.
28 S. L. Dexheimer, *Terahertz Spectroscopy: Principles and Applications*, CRC Press, New York, 2007.
29 J. A. Nóvoa, I. Ordóñez, C. Rial, J. Martín, A. Gil and J. R. Salgueiro, *J. Phys.: Conf. Ser.*, 2015, **605**, 012026.

